Research Article | Vol. 28, No. 4 / 17 February 2020 / Optics Express 5866
Optics EXPRESS

Influence of the pump scheme on the output power and the intensity noise of a single-frequency continuous-wave laser

YONGRUI GUO,[1] WEINA PENG,[1] JING SU,[1,2] HUADONG LU,[1,2,*] AND KUNCHI PENG[1,2]

[1]State Key Laboratory of Quantum Optics and Quantum Optics Devices, Institute of Opto-Electronics, Shanxi University, Taiyuan 030006, China
[2]Collaborative Innovation Center of Extreme Optics, Shanxi University, Taiyuan, Shanxi 030006, China
*luhuadong@sxu.edu.cn

Abstract: The influence of the pump scheme on the intensity noise of the single-frequency continuous-wave (CW) laser is investigated in this paper, which is implemented in a single-frequency CW Nd:YVO_4 1064 nm laser by comparing the traditional 808 nm pumping scheme (TPS) to the direct 888 nm pumping scheme (DPS). Under the conditions that the lasers with TPS and DPS have the same cavity structure and the cavity mirrors, as well as the same operation state including the thermal lens of the laser crystals and the mode-matching between the pump laser mode and the laser cavity mode at the laser crystals, the output power of the laser with DPS is up-to 32.0 W, which is far higher than that of 21.1 W for the laser with TPS. However, the intensity noise of the DPS laser including resonant relaxation oscillation (RRO) frequency of 809 kHz, RRO peak amplitude of 31.6 dB/Hz above the shot noise level (SNL) and the SNL cutoff frequency of 4.2 MHz, respectively, is also higher than that of 606 kHz, 20.4 dB/Hz and 2.4 MHz for the TPS laser. After further analyses, we find that the laser crystal with high doping concentration and long optical length is employed for DPS laser in order to improve the pump laser absorption efficiency, which can simultaneously increase the dipole coupling between the active atoms and the laser cavity, and then results in a high RRO frequency with a large amplitude peak as well as a high SNL cutoff frequency of the laser.

© 2020 Optical Society of America under the terms of the OSA Open Access Publishing Agreement

1. Introduction

Single-frequency continuous-wave (CW) high power all-solid-state 1064 nm laser with perfect beam quality, high stability and low intensity noise has attracted rising interest in recent years owing to its extensive applications in the advanced fields of quantum information and quantum communication [1], atom cooling [2], precision measurements [3]. However, high power single-frequency solid-state lasers suffer from the resonant noises around the resonant relaxation oscillation (RRO) frequency, which comes from the interplay between the population inversion and the intracavity photons and delays the frequency of the laser reaching the shot noise level (SNL) frequency. Especially, when the high-power single-frequency CW solid-state laser is used as the pump source of multipartite entangled or squeezed lights, the magnitude of RRO noise can reduce the level of the squeezed and entangled lights in the frequency range from hundred kilohertz to several megahertz. Presently, the most popular way to achieve the low noise high power single-frequency laser is the laser amplification including the master oscillator power amplifier [4] and the injection-locked amplifier [5]. However, it is a pity that the intensity noise of the solid-state amplifier at high frequency close to the SNL can also be amplified accompanied by the power amplification and the noise eaters including the mode cleaners [6] and optoelectronic feedback schemes [7] have to be employed to filter the noise. Compared to the amplifier, high power operation of a single-frequency CW laser can be achieved in a single

#387392 https://doi.org/10.1364/OE.387392
Journal © 2020 Received 6 Jan 2020; revised 5 Feb 2020; accepted 5 Feb 2020; published 14 Feb 2020

Optics EXPRESS

laser resonator by optimizing the parameters of the laser resonator and choosing the suitable intracavity elements [8,9]. It is well known that the Nd:YVO_4 crystal is widely used as the laser crystal to generate the 1064 nm laser owing to its large stimulated emission cross-section [10]. In order to achieve the high optical conversion efficiency from the pump to the laser, the traditional 808 nm four-level pumping scheme (TPS) is broadly employed because the maximum absorption line of the Nd:YVO_4 crystal falls at 808 nm [11]. However, with the increase of the output power of the 1064 nm laser, a large challenge that we have to face to is the severe thermal effect and the thermal aberration of the Nd:YVO_4 crystal because of the large quantum defect between the 808 nm pump wavelength and the 1064 nm lasing wavelength and the large absorption coefficient difference between *a* and *c* axes of the vanadate laser crystal, which can harmfully narrow the stability working region (SWR) of the laser and then restrict the output power. In order to overcome the problem of the TPS, a direct 888 nm quasi-three-level pumping scheme (DPS) was adopted to increase the output power of the 1064 nm laser. The DPS laser at 888 nm has the intrinsic advantage of being immune to the polarization of the pump laser since the absorption coefficients on both *a* and *c* axes of the vanadate laser crystal at this pump wavelength are equal [12]. Moreover, a small Stokes shift of the DPS laser can considerably decrease the heat generation. Even though the absorption coefficient of vanadate crystal at 888 nm is low, the absorption efficiency can be compensated by increasing the doped concentration and lengthening the laser crystal, which is also useful to spread the heat load over a larger volume of the laser crystal and then reduce the thermal lens effect [13]. Therefore, the output power can be considerably increased because more pump power can be injected to the DPS laser resonator. In 2014, by combining the DPS and optimization of the ratio between the linear loss and nonlinear loss, a 33.7 W end-pumped single-frequency Nd:YVO_4 laser at 1064 nm was realized [14]. The optical power of the laser was further scaled to 50 W via increasing the pump power of the laser diode (LD) to 113 W together with optimizing the transmissivity of the output coupler to 25% on the basis of precisely measuring the intracavity linear loss by the nonlinear loss [8]. Recently, the maximum optical power of the single-frequency CW 1064 nm DPS laser has been scaled up-to 101 W by means of employing two identical end-pumped laser crystals to relax the thermal lens of the laser crystals and an imaging system to realize laser mode self-reproduction at the two laser crystals [9]. Up to now, there is few works reported about the influence of the pump scheme on the intensity noise properties of a single-frequency CW laser, to the best of our knowledge. Therefore, the influence of the pump scheme on the intensity noise characteristics of the single-frequency CW Nd:YVO_4 lasers at 1064 nm is focused and investigated in this paper. It is found that for the DPS, increasing the doped ion concentration and lengthening the laser crystal can simultaneously enhance the interaction between the inversion population and the intracavity photons, which can further contribute to the lasing relaxation oscillation and the amplification of the laser intensity noise.

2. Experimental setup

To implement the comparison of the influence of the pump scheme on the intensity noise of the laser, a bow-tie four-mirror unidirectional ring resonator with the resonant length of $L = 450$ mm is constructed in the experiment and depicted in Fig. 1. According to the requirements of TPS and DPS, two fiber-coupled LDs with center wavelengths of 808 and 888 nm with corresponding maximum pump powers of 51 and 80 W act as the pump source, respectively. The diameters and numerical apertures of both LDs are 400 μm and 0.22, respectively. The pump laser beam of each LD is focused to 1020 μm diameter spot and injected at the place of the laser crystal. In order to adequately absorb the pump laser, both corresponding laser crystals are a-cut composite YVO_4/Nd:YVO_4 rods. But one has an un-doped end cap of 5 mm and Nd-doped part of 15 mm with concentration of 0.2%, and the other has an un-doped end cap of 3 mm and Nd-doped part of 20 mm with the concentration of 0.8%. Both laser crystals have the same wedge angle of

Optics EXPRESS

1.5° at the rear end face to keep the stable polarization of the oscillating laser, and both of them are wrapped with indium foil and mounted in a temperature-controlled copper oven. The input coupling mirror M_1 is a concave-convex lens with the curvature of 1500 mm. The incident and output surfaces are coated with anti-reflectivity (AR) film at pump laser wavelength 808 and 888 nm ($R_{808nm,888nm}$<0.5%) and high-reflection (HR) film at 1064 nm (R_{1064nm}>99.7%), respectively. M_2 is a plane-convex mirror (R=1500 mm) coated with HR film at 1064 nm (R_{1064nm}>99.7%). M_3 and M_4 are both plane-concave mirrors with the curvature radius of 100 mm (R=-100 mm). M_3 is also coated with HR film at 1064 nm (R_{1064nm}>99.7%). The output coupling mirror M_4 is coated with partial transmission of T=20% at 1064 nm. An optical diode comprised by a half-wave plate (HWP) and an 8 mm-long terbium gallium garnet (TGG) crystal mounted in a hollow cylindrical permanent magnet is employed to eliminate the spatial hole-burning effect and achieve the stable unidirectional operation of the laser. In addition, sufficient nonlinear loss is introduced to the resonator by a type-I non-critically phase-matched lithium triborate (LBO) crystal (S1, S2: $AR_{1064nm;532nm}$) [15] with the temperature controlled by a homemade temperature-controller with a precision of 0.01 °C to ensure the stable single-frequency operation of the laser. The LBO crystal has a dimensions of 3 mm × 3 mm × 18 mm and been placed at the beam waist between mirrors of M_3 and M_4. The launched 532 nm beam from the attained single-frequency CW laser is separated from the main 1064 nm laser beam with a dichroic mirror and measured by a power meter (PM_1: LabMax-Top, Coherent) with an uncertainty of ±1%.

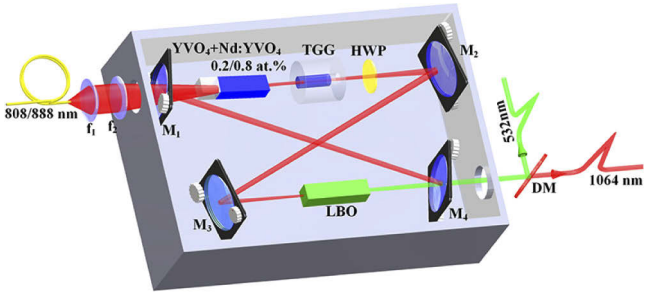

Fig. 1. Schematic diagram of the designed laser. TGG, terbium gallium garnet; LBO, lithium triborate; HWP, half-wave plate; f_{1-2}, lens; DM, dichroic mirror.

The experimental setup for measuring the intensity noise of the laser is illustrated in Fig. 2. Most part of the 1064 nm laser is reflected into another power meter (PM_2: LabMax-Top, Coherent) by the mirror S_1. The leaked laser beam from S_1 is divided into two parts by the mirror S_2. One part is directly injected into a scanned confocal Fabry-Perot cavity with the assist of a lens f_3 to monitor the longitudinal-mode structure of the laser. The free spectral range and finesse of the adopted Fabry-Perot (F-P) cavity are 750 MHz and 140, respectively. The other part is equally divided into two parts again by a 50/50 beam splitter composed of another HWP and a polarization beam splitter (PBS). The power of each laser beam is controlled to 1 mW. S_3, S_4 and f_4, f_5 are used to align and focus both laser beams into the balanced homodyne detector (BHD). The output signal of the BHD is recorded by a spectrum analyzer with the resolution bandwidth (RBW) of 30 kHz and video bandwidth (VBW) of 30 Hz. The intensity noise measurements and data processing of the measured results are the same as those demonstrated in our previous literature [8].

Optics EXPRESS

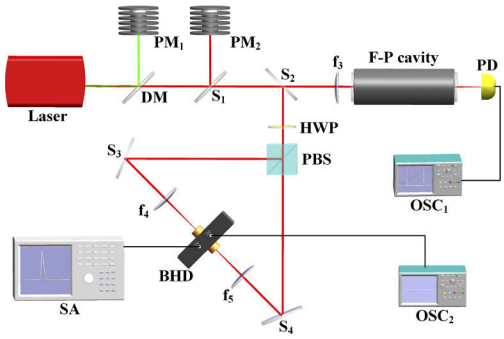

Fig. 2. Schematic diagram of the experimental setup. PBS, polarization beam splitter; BHD, balanced homodyne detector; OSC_{1-2}, digitizing oscilloscope.

3. Experimental results and analyses

In the experiment, the temperature of the LBO crystal is firstly controlled to room value of 25 °C, which is beneficial for directly investigating the influence of the pump scheme on the intensity noise of the attained single-frequency 1064 nm laser. In this case, only the 1064 nm laser beam can leak from the laser resonator and the output power of 1064 nm laser with TPS and DPS as the function of the absorbed pump power at 808 and 888 nm wavelength is shown in Fig. 3. It can be seen that the threshold power and maximum output power of the laser are 31.40±0.31 and 21.11 ±0.21 W for the TPS, respectively. For the DPS, the threshold of the laser is 30.60±0.31 W, which is similar to that of the TPS. However, the maximum output power can reach up to 32.00±0.32 W with the absorbed pump power of 71.20±0.71 W. The optical conversion efficiencies of the TPS and DPS lasers are 42.2% and 45.0%, respectively, with respect to the pump absorption efficiencies of 98% and 89% at the highest incident pump powers of 51.00±0.50 and 80.00±0.80 W for the two lasers, respectively. In curves (a) and (b) of Fig. 3, the slope efficiencies of both TPS and DPS lasers are low at the absorbed pump power below 40.00±0.40 W. On the one hand, the laser works at the edge of the SWR at this moment, which results in a poor mode-matching between the pump and lasing beam at the central of the laser crystal. On the other hand, the difference between the emission wavelength of the LD at low pump power and the absorption line of the laser crystal leads to a low pump absorption efficiency. Once the absorbed pump power is beyond 40.00±0.40 W, the severe thermal lens effect of the TPS laser can not only make the laser quickly enter the SWR and achieve the optimal mode matching but also quickly jump out of the SWR. Consequently, the output power of the laser is restricted to 21.10±0.21 W. Contrary to the TPS laser, the relatively smaller thermal lens effect of the DPS laser can delay the laser to reach optimal mode matching from entering the SWR. Therefore, a smaller slope efficiency of the output power curve is observed for the DPS laser. In this case, it is a pleasure that more pump power can be easily injected into the resonator to further scale up the output power. As a result, the output power of DPS laser can be scaled up to 32.00±0.32 W when the incident pump power is increased to 80.00±0.80 W. When taking into account the thermal loads of η_{ht}=25% and η_{hd}=17% of the laser crystals for lasers with the TPS and DPS, the corresponding thermal focal lengths of the laser crystals [16]

$$f_{th} = \frac{\pi K \omega_p^2}{\eta_h P_p \eta_{abs} dn/dT}, \tag{1}$$

(where K is the thermal conductivity of the laser crystal, ω_p is the beam waist radius of pump laser, dn/dT is the thermooptic coefficients of the refractive index n, $P_p * \eta_{abs}$ is the absorbed pump power, where η_{abs} is the absorption efficiency of the pump laser) are calculated to be 122.4

Optics EXPRESS

and 126.3 mm, respectively, with respect to the laser beam waist radii of about 370 and 340 μm at the central of the two laser crystals, respectively. The pump-to-mode size ratios of about 1.37 and 1.50 for the achieved 1064 nm lasers with TPS and DPS satisfy the mode-matching condition presented by Chen [17], which reveals that the two lasers almost have the same operation state.

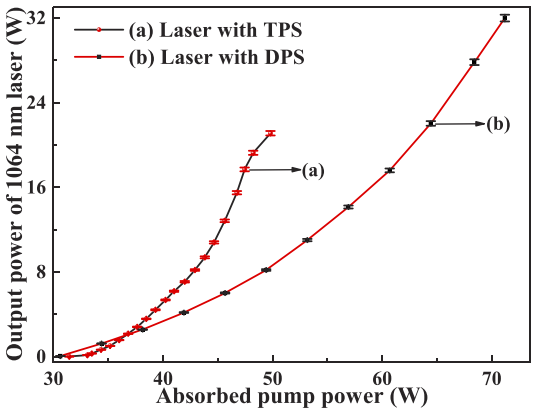

Fig. 3. Output power of the 1064 nm laser versus the incident pump power.

Then the intensity noise spectrum of the 1064 nm laser under single-frequency operation is measured with the BHD and depicted by the relative intensity noise (RIN). For comparison, we normalize the intensity noise spectrum of the DPS laser to that of the TPS laser according to the normalizing equation [18]

$$V_{obs} = 1 + \chi(V_n - 1), \tag{2}$$

where V_{obs} and V_n are observed and normalized intensity noise spectra, respectively, the χ is the normalizing factor which equals the ratio between the maximum output powers of the DPS laser to that of the TPS laser. Figure 4 illustrates the RIN spectra of the TPS and DPS lasers. It can be found that the RRO frequency, the RRO peak amplitude above the SNL, and the SNL cutoff frequency of the TPS laser are 606 kHz, 20.4 dB/Hz, and 2.6 MHz, respectively. However, for the DPS laser, the corresponding values are lifted to 809 kHz, 31.6 dB/Hz, and 4.2 MHz, respectively. From the results, we can also conclude that the increase of the output power for the DPS is accompanied by the elevation of the intensity noise. We further analyze the reason for the intensity noise spectrum difference between the TPS and DPS lasers. The intensity noise spectrum of a single-frequency laser at fundamental wave (FW) can be given by [19]

$$\begin{aligned} V_f = {} & k_1(\omega_f, \gamma_f)V_{vac} + k_2(\omega_f, \gamma_f)V_p + k_3(\omega_f, \gamma_f)V_{spont} \\ & + k_4(\omega_f, \gamma_f)V_{dipole} + k_5(\omega_f, \gamma_f)V_{losses}, \end{aligned} \tag{3}$$

where k_1, k_2, k_3, k_4, and k_5 are the coefficients with respect to the vacuum noise V_{vac} caused by the output coupler, V_p the noise coming from the pump source, V_{spont} the noise coming from spontaneous-emission, V_{losses} the noise induced by the intracavity losses, and V_{dipole} the noise caused by dipole fluctuations, respectively. ω_f and γ_f [19] are the RRO frequency and the damping rate of the oscillation for V_f, respectively. The key parameters in k_1, k_2, k_3, k_4, and k_5 of both lasers are listed in Table 1. Wherein except the pump noise V_p is the measured relative intensity noise value, the other parameters are the calculation results of the corresponding lasers. It has verified that the dominant contributors to the magnitude of the RRO peak are the vacuum fluctuation, dipole fluctuation, and the noise caused by the intracavity loss [19,20]. Below and beyond the RRO frequency, the main contributors are the pump noise and the vacuum fluctuation, respectively [19,20]. From Table 1, it can be seen that the measured pump noise V_p (1 mW)

Optics EXPRESS

of 12.80±0.17 dB for the DPS laser injected with maximum pump power of the 888 nm LD is higher than that of 7.60±0.19 dB for the TPS laser pumped with maximum pump power of the 808 nm LD. The high pump noise can contribute to a high tensity noise of the DPS laser below the frequency of RRO. For the RRO peak, since there are the same intracavity loss as well as the transmission of the output coupling mirror for both lasers, the larger amplitude of the RRO peak for the DPS laser than that of the TPS laser can be ascribed to stronger dipole fluctuations. The dipole fluctuation of a laser comes from the dipole coupling between the atoms and the laser resonator, which is determined by the number of the stimulated atoms N [21]. The laser with DPS, matched with a high doping concentration and long length laser crystal for improving the pump laser absorption efficiency of the laser, has the atoms N of about 5.3 times larger than that of the TPS laser. On this basis, large stimulated emission rate G [21] for the laser with DPS can further enhance this dipole coupling between the atomic transition and cavity lasing modes. From Table 1, we can see that the stimulated radiation rate G of the DPS laser is also about 5.3 times larger than that of the TPS laser. The high RRO frequency and RRO peak simultaneously delays the frequency to the SNL and directly induces the SNL cutoff frequency of the DPS laser up to 4.2 MHz. Above analyses can be further verified by taking the parameters in Table 1 into the Eq. (3), theoretical simulations of the intensity noise spectra for laser with TPS and DPS are with respect to the curve (a) and curve (b) shown in Fig. 5, respectively. In Fig. 5, the theoretical simulations results of the amplitude and frequency of the RRO peak for the TPS laser are 39.3±0.2 dB/Hz above the SNL and 615±2 kHz, which are lower than that of the 43.9±0.2 dB/Hz above the SNL and 807±2 kHz for the DPS laser. The high RRO peak simultaneously delays the frequency to the SNL and directly induces the SNL cutoff frequency of the DPS laser up to 4.5±0.1 MHz, which is also higher than that of 2.7±0.1 MHz for the TPS laser. It is clear that the trend of the theoretical simulations can consist with the presented experimental results. In a word, compared to the TPS laser, the output power of the single-frequency CW laser can be effectively improved by employing the DPS, but the intensity noise from the low to high frequencies is also elevated.

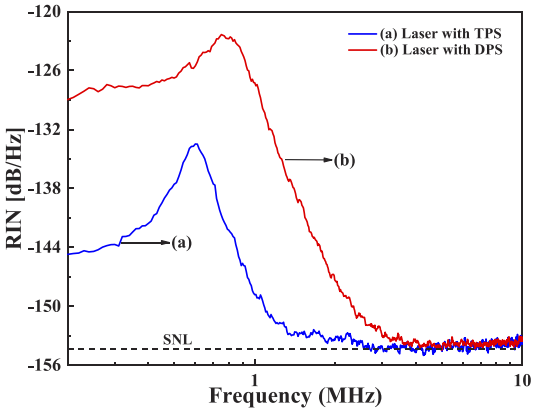

Fig. 4. Intensity noise spectra of the single-frequency laser without the nonlinear loss.

At last, by matching LBO crystal to the optimal phase-matching temperature of 148 °C, the nonlinear loss was introduced into the laser resonator to further suppress the intensity noise of the two lasers [22]. The output power for the TPS and DPS lasers are shown in picture (a) and (b) of Fig. 6, respectively. With respect to the nonlinear loss of η=1.10% and η=1.22% for the TPS and DPS lasers, the output power of the two lasers at 1064 and 532 nm are 19.90±0.20 and 1.10±0.01 W, and 29.60±0.30 and 1.80±0.02 W, respectively. The nonlinear loss η is defined by the ratio between the power of 532 nm laser and that of the intracavity 1064 nm laser [22]. The measured RIN spectra of the two lasers depicted in Fig. 7 show that the nonlinear loss is

Optics EXPRESS

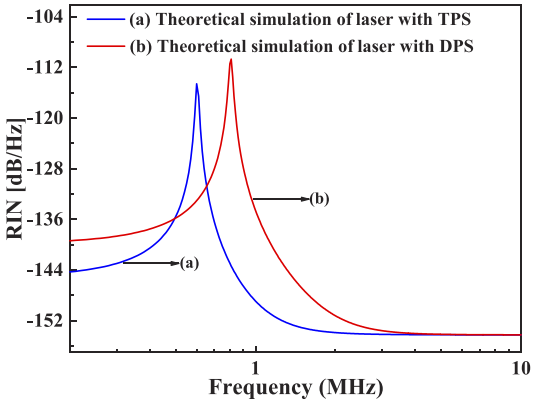

Fig. 5. Theoretical simulation of the intensity noise spectra for the lasers with TPS and DPS.

Table 1. Parameters for 1064 nm lasers with TPS and DPS

Parameter	Laser with TPS	Laser with DPS
V_p (dB)	7.60±0.19	12.80±0.17
N (atoms)	$(3.09\pm0.44)\times10^{17}$	$(1.65\pm0.06)\times10^{18}$
G (s^{-1})	$(3.28\pm0.47)\times10^{10}$	$(1.75\pm0.06)\times10^{11}$
ω_f (kHz)	615±2	807±2
γ_f (s^{-1})	$(102\pm5)\times10^3$	$(168\pm5)\times10^3$

useful to suppress the RRO peak. With the assist of the nonlinear loss, the RRO peak for both TPS and DPS lasers are easy to be wiped up. However, the intensity noise below the RRO peak and the intensity noise cutoff frequency is immune to the nonlinear loss. Figure 8 depicts the representative longitudinal-mode structure of the laser, which illustrates that both lasers can work with stable single-frequency operation with the assistance of the nonlinear loss.

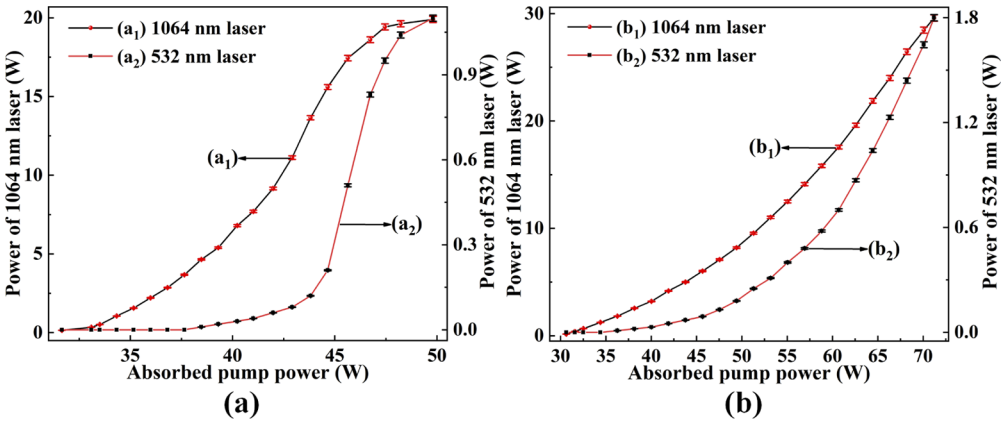

Fig. 6. Output power of the laser with the nonlinear loss. (a) Output power of the laser with TPS; (b) output power of the laser with DPS.

Optics EXPRESS

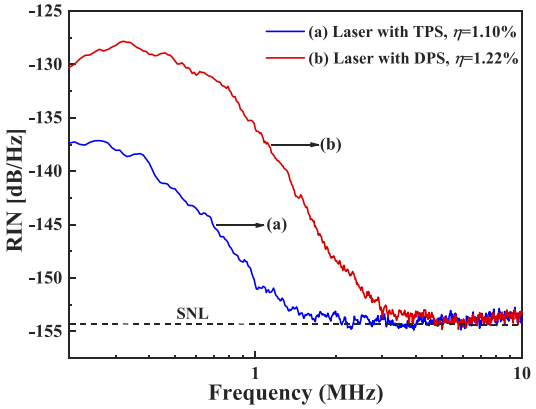

Fig. 7. Intensity noise spectra of the single-frequency laser with the nonlinear loss.

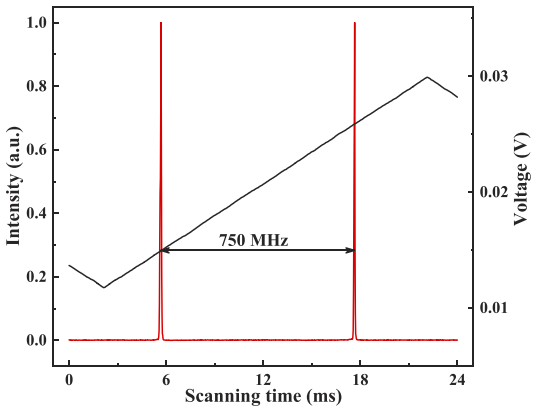

Fig. 8. Measured single-longitudinal-mode structure of the laser.

4. Conclusions

In summary, the influence of the pump scheme on the intensity noise of single-frequency CW lasers is investigated in this paper. Because of the different thermal lens effect of the laser crystal for TPS and DPS, the output power of the single-frequency CW laser is scaled up from 21.1 W to 32.0 W when the TPS is replaced by the DPS. However, it is a pity that the increase of the output power is accompanied by the elevation of the intensity noise for the DPS. From the measured results, it is found that the RRO frequency, the amplitude of RRO peak above the SNL as well as the SNL cutoff frequency are increased from 606 kHz, 20.4 dB/Hz, and 2.4 MHz to 809 kHz, 31.6 dB/Hz, and 4.2 MHz after replacing the TPS with the DPS. The high intensity noise of the DPS below the frequency of RRO peak results from the high pump noise caused by the high pump power. Moreover, in order to improve the absorption efficiency of the pump light for the DPS laser, the laser crystal with high doping concentration and long optical length is utilized in the experiment, which can not only enhance the dipole coupling between the large amount atoms and the laser cavity and increase the dipole fluctuation, but also increase the stimulated radiation rate G. Eventually, both the RRO peak of the DPS laser including the frequency as well as amplitude peak and the SNL cutoff frequency are higher than that of the TPS laser. Both the intensity noise of the lasers with TPS and DPS below the frequency of RRO can be further reduced by controlling the pump laser noise with optoelectronic feedback schemes. We believe

Optics EXPRESS

that the work can supply a good reference for designing a single-frequency CW laser with good performance to meet different application requirements. The DPS can be employed to obtain a single-frequency laser with a high output power as well as TPS combined with a controlled laser crystal doping concentration can be utilized to achieve a single-frequency laser with a low intensity noise.

Funding

National Key Research and Development Program of China (2017YFB0405203).

Disclosures

The authors declare no conflicts of interest.

References

1. S. L. Braunstein and P. Van Loock, "Quantum information with continuous variables," Rev. Mod. Phys. **77**(2), 513–577 (2005).
2. D. J. Wineland and W. M. Itano, "Laser cooling of atoms," Phys. Rev. A **20**(4), 1521–1540 (1979).
3. LIGO scientific collaboration and Virgo collaboration, "Observation of gravitational waves from a binary black hole merger," Phys. Rev. Lett. **116**(6), 061102 (2016).
4. M. Frede, B. Schulz, R. Wilhelm, P. Kwee, F. Seifert, B. Willke., and D. Kracht, "Fundamental mode, single-frequency laser amplifier for gravitational wave detectors," Opt. Express **15**(2), 459–465 (2007).
5. L. Winkelmann, O. Puncken, R. Kluzik, C. Veltkamp, P. Kwee, J. Poeld, C. Bogan, B. Willke, M. Frede, J. Neumann, P. Wessels, and D. Kracht, "Injection-locked single-frequency laser with an output power of 220 W," Appl. Phys. B **102**(3), 529–538 (2011).
6. B. Willke, N. Uehara, E. K. Gustafson, R. L. Byer, P. J. King, S. U. Seel, and R. L. Savage Jr., "Spatial and temporal filtering of a 10-W Nd:YAG laser with a Fabry–Perot ring-cavity premode cleaner," Opt. Lett. **23**(21), 1704–1706 (1998).
7. B. C. Buchler, E. H. Huntington, C. C. Harb, and T. C. Ralph, "Feedback control of laser intensity noise," Phys. Rev. A **57**(2), 1286–1294 (1998).
8. Y. R. Guo, H. D. Lu, M. Z. Xu, J. Su, and K. C. Peng, "Investigation about the influence of longitudinal-mode structure of the laser on the relative intensity noise properties," Opt. Express **26**(16), 21108–21118 (2018).
9. Y. R. Guo, M. Z. Xu, W. N. Peng, J. Su, H. D. Lu, and K. C. Peng, "Realization of a 101 W single-frequency continuous wave all-solid-state 1064 nm laser by means of mode self-reproduction," Opt. Lett. **43**(24), 6017–6020 (2018).
10. http://www.castech.com/manage/upfile/fileload/20170824170727.pdf.
11. J. Q. Zhao, Y. Z. Wang, B. Q. Yao, and Y. L. Ju, "High efficiency, single-frequency continuous wave Nd:YVO_4/YVO_4 ring laser," Laser Phys. Lett. **7**(2), 135–138 (2010).
12. L. McDonagh, R. Wallenstein, R. Knappe, and A. Nebel, "High-efficiency 60 W TEM_{00} Nd:YVO_4 oscillator pumped at 888 nm," Opt. Lett. **31**(22), 3297–3299 (2006).
13. L. McDonagh, R. Wallenstein, and A. Nebel, "111 W, 110 MHz repetition-rate, passively mode-locked TEM_{00} Nd:YVO_4 master oscillator power amplifier pumped at 888 nm," Opt. Lett. **32**(10), 1259–1261 (2007).
14. H. D. Lu, J. Su, Y. H. Zheng, and K. C. Peng, "Physical conditions of single-longitudinal-mode operation for high-power all-solid-state lasers," Opt. Lett. **39**(5), 1117–1120 (2014).
15. H. D. Lu and K. C. Peng, "Realization of the single-frequency and high power as well as frequency-tuning of the laser by manipulating the nonlinear loss," J. Quantum Opt. **21**(2), 171–176 (2015).
16. Y. J. Wang, Y. H. Zheng, Z. Shi, and K. C. Peng, "High-power singlefrequency Nd:YVO_4 green laser by self-compensation of astigmatisms," Laser Phys. Lett. **5**(7), 506–509 (2008).
17. Y. F. Chen, "Pump-to-mode size ratio dependence of thermal loading in diode-end-pumped solid-state lasers," J. Opt. Soc. Am. B **17**(11), 1835–1840 (2000).
18. C. C. Harb, T. C. Ralph, E. H. Huntington, I. Freitag, D. E. McClelland, and H. A. Bachor, "Intensity-noise properties of injection-locked lasers," Phys. Rev. A **54**(5), 4370–4382 (1996).
19. C. C. Harb, T. C. Ralph, E. H. Huntington, D. E. McClelland, and H. A. Bachor, "Intensity-noise dependence of Nd:YAG lasers on their diode-laser pump source," J. Opt. Soc. Am. B **14**(11), 2936–2945 (1997).
20. T. C. Ralph, C. C. Harb, and H. A. Bachor, "Intensity noise of injection-locked lasers: Quantum theory using a linearized input-output method," Phys. Rev. A **54**(5), 4359–4369 (1996).
21. J. Zhang, K. S. Zhang, Y. L. Chen, T. C. Zhang, C. D. Xie, and K. C. Peng, "Intensity noise properties of LD pumped single-frequency ring lasers," Acta Optic Sin. **20**(10), 1311–1316 (2000).
22. H. D. Lu, Y. R. Guo, and K. C. Peng, "Intensity noise manipulation of a single-frequency laser with high output power by intracavity nonlinear loss," Opt. Lett. **40**(22), 5196–5199 (2015).

218.26.34.71 on 09/2021 03:22:09 46.307